Energy & Environmental Science

ROYAL SOCIETY OF CHEMISTRY

PAPER

View Article Online
View Journal | View Issue

Cite this: *Energy Environ. Sci.*, 2021, **14**, 916

Post-combustion emissions control in aero-gas turbine engines†

Prakash Prashanth, Raymond L. Speth, Sebastian D. Eastham, Jayant S. Sabnis and Steven R. H. Barrett *

Emissions of nitrogen oxides (NO_x) from aircraft cause air quality degradation and climate change. Efforts to improve the efficiency of aircraft propulsion systems are leading to small, power-dense engine cores with higher overall pressure ratios and combustion temperatures, which can result in higher NO_x emissions. The trend towards smaller engine cores with smaller mass flow rates in the core stream, presents new opportunities for emissions control. Specifically, we propose and assess using a selective catalytic reduction (SCR) system that was previously infeasible when mass flow rates in the core were an order of magnitude larger than heavy-duty diesel engines for road based applications. SCR systems would reduce NO_x emissions at the cost of increased aircraft weight and specific fuel consumption due to the pressure drop in the core stream induced by the catalyst. We quantify the effects of these trade-offs in terms of emissions reduction and fuel burn increase using representative engine cycle models provided by a major aero-gas turbine manufacturer. Due to its size, any SCR system will likely need to be housed in the aircraft body, potentially making it most suitable for future hybrid- or turbo-electric aircraft designs. Furthermore, SCR systems require ultra-low sulfur (ULS) fuel to prevent catalytic fouling. We find that employing an ammonia-based SCR results in an approximately 95% reduction in NO_x emissions in exchange for a ~0.5% increase in block fuel burn. The performance of the post-combustion emissions control (PCEC) system is shown to improve for smaller-core engines, such as those proposed in the NASA *N* + 3 time-line (2030–2035). Using a global chemistry-transport model we estimate that PCEC used with ULS fuel, could avert ~92% of aviation air pollution related early deaths each year. Using a simplified climate model and accounting for changes in emissions (including life cycle emissions) and radiative forcing we estimate that PCEC with ULS fuel increases climate damages by ~7.5%. We estimate that the net benefit of using PCEC accounting for air quality and climate impacts is 304 USD (2015) per metric tonne of jet fuel burned, or a reduction of ~52% in monetized air quality and climate damages.

Received 24th July 2020,
Accepted 23rd November 2020

DOI: 10.1039/d0ee02362k

rsc.li/ees

Broader context

Emissions of nitrogen-oxides (NO_x) from the aviation industry have an impact on global climate change and air quality. It is well documented that NO_x is a precursor to fine particulate matter and ozone, which have an adverse impact on human health. The continued growth of the aviation industry will further increase the absolute and relative contribution of aviation emissions to global pollution. Moreover, the current techniques used to reduce NO_x emissions from aero-gas turbine engines are approaching their limit. Leveraging the trends in aircraft engine design and novel aircraft configurations such as turbo-electric designs, our work is the first proposal and assessment of post-combustion emissions control methods for aircraft gas turbine engines for a future commercial aircraft. Our findings indicate that using post-combustion emissions control can virtually eliminate aviation related air-quality damages at the cost of small increase in aviation climate impacts. While detailed investigations of various aspects and implications of post-combustion emissions control need to be undertaken, this work opens up a new area of study in the design of the next generation of aircraft and maybe a step towards the sustainable development of the aviation industry.

Laboratory for Aviation and the Environment, Department of Aeronautics and Astronautics, Massachusetts Institute of Technology, 77 Massachusetts Avenue, Cambridge, MA 02139, USA. E-mail: sbarrett@mit.edu

† Electronic supplementary information (ESI) available. See DOI: 10.1039/d0ee02362k

1 Introduction

Emissions of oxides of nitrogen (NO_x) adversely impact air quality and human health.[1,2] NO_x emitted at cruise altitude

produces ozone that upon reaching the surface alters the background chemistry to increase the concentration of fine particulate matter ($PM_{2.5}$). $PM_{2.5}$ and ozone cause asthma, cardiovascular, and respiratory diseases,[1,2] and increase risk of early death. Previous estimates (using 2006 data) suggest that NO_x emissions from global aviation results in $\sim$16 000 premature mortalities annually.[3] With the current growth rate of the aviation industry at an average of 5% per year,[4] the absolute and relative contribution of aviation NO_x emissions to air pollution is likely to increase over the coming decades. Furthermore, local air quality degradation near airports inhibits airport expansion. NO_x also has an impact on the climate, causing a short-term northern hemispheric warming effect on the order of aviation CO_2, with a long-term global cooling effect due to methane destruction.[5]

In the commercial aviation sector, gas turbines have been the primary choice of power plant since the early 1950s[6] due to their high power density (relative to reciprocating engines) and suitability for high subsonic speeds. The thermodynamic efficiency of the gas turbine increases with higher overall pressure ratio (OPR). A higher OPR leads to increased thermal NO_x production as the compressor exit temperature increases with OPR.[7] Various combustor design strategies such as RQL (rich-quench-lean) combustion chambers have provided $\sim$50% reduction in NO_x emissions compared to annular combustors[8] but their effectiveness decreases as OPR of the engines increase.[9] We propose that post-combustion treatment of the NO_x emissions could offer a solution by eliminating $>$90% NO_x emissions. It may also expand the design space for new engine architectures by partly decoupling combustor design from NO_x control.

1.1 Post-combustion emissions control in other industries

Heavy-duty diesel engines and the power generation industry routinely use post-combustion emissions control to reduce their emissions. NO_x emissions from aero-derivative engines (used for power generation) are approximately an order of magnitude lower than the original engines used in an aircraft.[8] This is in part due to the choice of fuel. A liquid fuel will result in local regions of stoichiometric conditions as the fuel droplets evaporate,[10] resulting in local high temperature pockets, that increase NO_x formation whereas natural gas used in ground-based power plants tends to lead to lower NO_x emissions.[8] However, the bulk of the emission reduction in ground-based power plants (over 90%) comes from post-combustion emissions control that is primarily in the form of selective catalytic reduction (SCR).

Prior to 1991, diesel engines in automobiles in the United States (US) did not require after-treatment and the average engine out NO_x emissions were 4.6 g kW^{-1} h^{-1}. By 2013 emissions regulations required all on-road engines in the US to use after-treatment measures to control emissions. The average NO_x emissions from diesel engines was reduced to 0.27 g kW^{-1} h^{-1} [11] over 20 years using SCR. This corresponds to approximately a 94% reduction in NO_x emissions. SCR systems in modern engines remove 95% to 98%[12] of NO_x across the catalyst.

1.2 Selective catalytic reduction (SCR)

SCR converts oxides of nitrogen (NO and NO_2) to N_2 and H_2O in the presence of a catalyst using an ammonia based reducing agent. The following section describes the reaction pathways and characteristics of the catalysts used.

1.2.1 SCR pathway. The two main reactions for the reduction of NO_x are:[13,14]

$$4NO + 4NH_3 + O_2 \rightarrow 4N_2 + 6H_2O$$

$$NO + NO_2 + 2NH_3 \rightarrow 2N_2 + 3H_2O$$

Greater than 90% of NO_x emissions from typical diesel engines (and gas turbines) consists of NO.[13] Since gas turbine emissions are also predominantly NO (approximately 95%),[15] except at low thrust conditions[16] as used in approach and taxi operations, the first of the two reactions is the primary reaction for deNO_x (conversion of NO_x to N_2 and H_2O) with ammonia.[13]

1.2.2 SCR catalysts and substrates. Different catalytic materials are used in SCR depending on the application. Platinum group metals (PGM) are used in lower temperature (175–250 °C) applications, while vanadium and titanium oxides are used at higher temperatures (300–450 °C).[17] Recent work has been focused on zeolite based catalysts, which have a broader operating temperature range (150–600 °C), higher conversion efficiency and are cheaper than PGM catalysts.[17,18] Monolithic catalysts are extruded cordierites with a catalytic wash-coat, the straight channels of these monoliths reduce the pressure drop associated with the flow through the channels. Cellular monolithic catalysts are chosen for this work due to the reduced pressure losses. Ref. 19 provides relevant properties of monolithic catalysts.

1.2.3 Reducing agents. The reducing agents used for the SCR reactions are ammonia based solutions.[12] A urea solution (marketed as AdBlue or Diesel Engine Fluid) is used by mobile SCR systems on-road. Urea solutions are used (instead of pure ammonia) for on-road applications in part due to safety concerns over handling pressurized pure anhydrous liquid ammonia. During the SCR process the ammonia based reducing agent is injected into the exhaust stream which then evaporates and mixes with the gas upstream of the catalyst. Properties of the reducing agents are given in Table 1.

1.2.4 Sulfur content and catalyst fouling. A consideration in the use of SCR is that sulfur content in the fuel can lead to catalyst fouling, which results in the deactivation of the catalytic sites and subsequent loss of catalytic performance. To prevent sulfur fouling and maintain catalytic performance, low sulfur fuel is required ($<$15 ppm) as is the case with ultra-low sulfur (ULS) diesel that is used on road vehicles.[21] Quantification of the environmental impacts and costs of desulfurizing jet fuel has been previously carried out by Barrett *et al.*[22] The scenario of interest considered in the subsequent sections with post-combustion emissions control (PCEC) will use ultra-low sulfur fuel (ULS).

1.3 Challenges to implementing SCR on aircraft engines

Implementing SCR on aircraft engines will result in increased pressure drop in the core air stream, and aircraft fuel consumption

Table 1 Properties of reducing agents.[20] AdBlue is a commercially used 32.5% urea solution for diesel engines. X_{m,NH_3} represents the moles of NH_3 contained in one kilogram of the reductant.[20] The fuel-specific reductant consumption (FSRC) is calculated for an assumed cruise emissions index, EI(NO_x) of 14 g kg^{-1} fuel. $\dot{m}_{Red}$ and $\dot{m}_f$ are the reductant mass flow rate and fuel mass flow rate, respectively

Reducing agent	Molecular formula	Density	X_{m,NH_3}	(FSRC) $\frac{\dot{m}_{Red}}{\dot{m}_f}$
—	—	(kg m^{-3})	(mol NH_3 per kg reductant)	(g reductant per kg fuel)
AdBlue	$(NH_2)_2CO$ + H_2O	1086	10.8	28.1
Solid urea	$(NH_2)_2CO$	1330	33.3	9.14
Anhydrous liquid ammonia	NH_3	610	58.7	5.18

is sensitive to such a pressure drop. The mass flow rates through the core of a gas turbine engine used to power an Airbus A320 size aircraft during cruise is 25–30 kg s^{-1} (based on cycle calculations and ref. 23). This is the mass flow that needs to be treated by the catalyst. For comparison, a heavy-duty diesel engine has a mass flow rate on the order of 1 kg s^{-1} (calculated at peak power for 4 stroke engines such as the Paccar MX13[24]). The higher mass flow rate in an aircraft engine increases the deleterious effect of a pressure drop in the core stream. The ideal operating temperature range for ion-exchanged zeolite SCR catalysts is approximately 550–650 K.[25] This temperature range generally occurs after the low pressure turbine (LPT) for the engine class under consideration. Installing a catalyst downstream of the LPT will cause a pressure drop downstream of the turbine, thus reducing the work that it can extract. In order to maintain the required work output, the fuel flow to the engine needs to be increased from the baseline case (with no catalyst), thus increasing the thrust specific fuel consumption (SFC). Furthermore, aircraft fuel consumption is more sensitive to vehicle mass than is the case with road vehicles. In the past, these weight and SFC concerns had discouraged any investigation into the use of SCR in aircraft.[8]

Today the core size of the engine is becoming smaller in new engine architectures such as the Pratt and Whitney geared turbofan and proposed small core engines.[26] The smaller, power dense core implies that a smaller mass of exhaust gas needs to be treated for a fixed engine thrust. This reduces the impact of a pressure drop in the core stream on the engine SFC. Furthermore, these cores contribute little to the overall engine thrust. For example, approximately 8.0% of the gross thrust in the modeled geared turbofan comes from the core exhaust and we estimate that for a small core engine as described by Lord *et al.*[26] the core flow will contribute 3.6% of the gross thrust.

Approaches designed to improve engine efficiency such as increased pressure ratios also increase NO_x emissions. Present low-NO_x combustor designs, which attempt to change the flame structure within the combustor to reduce residence time in high temperature regions[9] will be less effective as the OPR increases.[9] Post-combustion emissions control could provide an alternative approach.

Efforts to improve the overall efficiency of the aircraft have led to novel architectures and configurations. For example propulsion, airframe integration, distributed propulsion, turbo-/hybrid-electric propulsion, and boundary layer ingestion. The work done in these areas have been primarily aimed at improving the system level efficiency of the aircraft. These changes in configuration also present a new opportunity to implement an SCR based system to reduce the NO_x emissions from the engine. For example, an SCR based system could be used in a turbo-/hybrid-electric aircraft with fuselage embedded gas turbines, or mechanical transmission in other configurations.

This work quantifies the additional fuel burn (which is proportional to CO_2 emissions) incurred as a function of NO_x reduction relative to a baseline design. We evaluate the environmental costs and benefits of lower NO_x and increased CO_2 emissions by quantifying air quality and climate impacts. We include the life cycle emissions of CO_2 for the fuel (accounting for the desulfurization process) and ammonia (for SCR based post-combustion emissions control) in the analysis. The uncertainties in the analysis are propagated using a Monte Carlo approach, where feasible.

2 Methods

This section outlines the approach taken to evaluate the implementation of ammonia-based SCR of NO_x on aircraft gas turbine engines, which is detailed in subsequent subsections. After sizing the catalyst, we quantify the pressure drop through the catalyst and use an engine model to calculate the increase in SFC. We then calculate the increase in fuel burn from the baseline case due to the additional weight of the reducing agent and the catalyst and the increased SFC due to the pressure loss in the catalyst. Using global atmospheric modeling tools and the calculated reduction in NO_x we estimate the effect this has on ground level $PM_{2.5}$ and ozone concentrations. Air quality impacts are estimated using epidemiological studies that relate the health impacts to the change in exposure to $PM_{2.5}$ and ozone. Country-specific values of statistical life (VSL) are used to monetize the impacts. The changes in radiative forcing (RF) due to post-combustion emissions control are estimated using a radiative transfer model coupled to a global atmospheric chemistry-transport model. The changes in RF and CO_2 (due to increased fuel burn) are used to quantify the monetized climate impacts using a simplified climate model (Section 2.5.1). These costs and benefits are then aggregated to estimate the overall monetized impact of adopting post-combustion emissions control.

2.1 Mass transfer in monolithic catalyst and SCR model

The SCR process consists of bulk mass transfer, diffusion through the pores of the catalyst wash coat, followed by chemical reaction at the catalytic site. Each of these processes is temperature dependent – as the temperature increases, the chemical reaction rate increases exponentially[27] while the diffusion coefficients of the gas increases approximately with $T^{3/2}$,[27] where T is the temperature of the gas. Therefore, at sufficiently high temperatures ($T > 500$ K), the bulk diffusion or mass transfer becomes the limiting process.[14] This operating regime is referred to as the mass transfer-limited regime.

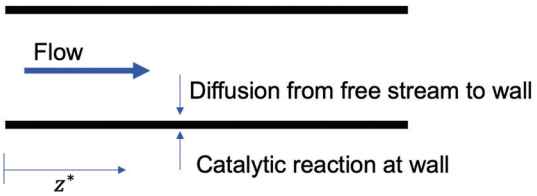

Fig. 1 Illustration of flow through a channel. The variable z^* represents the non-dimensional co-ordinate in the direction of flow, $z^* = (zD_{NO})/(ud^2)$, where D_{NO} is the diffusivity of NO, d is the hydraulic diameter of the channel, z is the axial distance and u is the local flow velocity.

In this section we describe a lumped parameter model of the monolithic reactor. Tronconi and Forzatti[28] showed the adequacy of lumped parameter models for simulating SCR reactors, finding an average error between experiments and the lumped one-dimensional model of 1.3%. In this model, average values of velocity and non-dimensional species concentration over the channel cross-section are used. The non-dimensional NO concentration is represented by $\Gamma = [NO]/[NO]_0$, where [NO] is the local concentration of NO and $[NO]_0$ is the concentration of NO at the inlet to the catalyst channel.

Based on the work done by Tronconi and Forzatti[28] we can express the efficiency of the catalyst in removing NO_x in the exhaust ($deNO_x$) as

$$deNO_x = 1 - \Gamma = \exp\left(-4\int_0^{z^*} \frac{DaSh}{Da + Sh} dz^*\right). \quad (1)$$

where $Sh(z^*)$ is the local Sherwood number, Da is the Damköhler number and z^* is the non-dimensional axial distance defined as $z^* = (zD_{NO})/(ud^2)$ as illustrated in Fig. 1. The Sherwood number represents the ratio of convective mass transfer to diffusive mass transfer, while the Damköhler number, represents the ratio of rate of chemical reaction of a species to the mass transfer rate, *i.e.* the ratio of the rate at which a species reacts at the catalyst wall to the rate at which the species is transported to the wall.

2.2 Pressure drop in monolithic catalysts

Installing an SCR catalyst downstream of the turbines introduces a pressure drop associated with the flow through a catalyst monolith. We estimate the pressure drop the fluid experiences with[29]

$$\Delta P = 4f\frac{l}{d} \times \frac{1}{2}\rho v^2,$$

where f is the Fanning friction factor, l is the length of the channel, d is the hydraulic diameter of the channel and $\frac{1}{2}\rho v^2$ is the dynamic pressure of the flow. If the flow regime is laminar (as is almost always the case[29]) then the friction factor $f = \frac{14.23}{Re}$ (for square channels), where $Re = \frac{\rho v d}{\mu}$, ρ is the density, μ is the dynamic viscosity, and v is the local flow velocity of the exhaust gas. The pressure loss associated with the inlet and outlet of the channel are estimated as

$$\Delta P_{in/out} = K_{in/out} \times \frac{1}{2}\rho v^2,$$

where $K_{in/out}$ is the inlet or outlet loss coefficients,[29] which are given by

$$K_{in} = -0.415 \times OFA + 1.08$$

and

$$K_{out} = (1 - OFA)^2,$$

where OFA refers to the open frontal area of the catalyst, *i.e.* the fraction of the frontal area that is open for the fluid to flow through.

2.3 Estimating the increase in SFC due to a pressure loss in the catalyst

A gas turbine cycle deck is used to estimate the increase in SFC due to the pressure loss through the catalyst monolith. In this work we use a GasTurb 13 engine model provided by Pratt and Whitney to evaluate the impact on SFC due to a pressure drop downstream of the LPT.

The implications for three engines were assessed, a representative turbofan (110 kN (25 000 lbf) thrust class), a geared turbofan for the same thrust class and a small core engine (58 kN (13 000 lbf) thrust class). The lower thrust of the small core engine reflects the lift to drag ratio ($L/D \approx 20$)[30] benefits from future airframes.

The effect of the pressure drop through the catalyst is modeled by varying the turbine exit duct pressure loss in a series of calculations. GasTurb was run iteratively such that the engine produces the same design point thrust for each turbine exit duct pressure drop by adjusting the combustor exit temperature. This corresponds to increasing the fuel flow rate and hence the SFC. The increase in the maximum landing mass and SFC, is used to calculate the percentage increase in fuel burn from eqn (2) as described in Section 2.4.

We size the catalyst by first considering effective bulk dimensions as shown in Fig. 2. The catalyst for this purpose is characterized by three parameters – the catalyst substrate, total frontal area (A) of the catalyst and the reacting length (l) of each channel in the catalyst. The catalyst substrate sets the hydraulic diameter of each channel, the bulk density and the open frontal area (OFA) of the catalyst. The total frontal area, A sets the local velocity of the flow in each channel by continuity and the reacting length of the channel sets the residence time of the exhaust gases within the catalyst.

The above three parameters also indirectly affect the SFC of the engine. Once values are chosen for the substrate, flow through area and the reacting length we compute the pressure drop and the NO_x conversion fraction. The pressure drop and additional weight is then used to calculate the increase in fuel burn from the baseline case (where no after-treatment is used and no additional weight is carried).

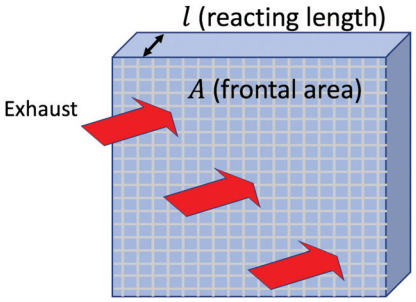

Fig. 2 Bulk effective dimensions of the lumped catalyst model. Frontal area is defined as the area perpendicular to the flow through the catalyst.

2.4 Estimating the fuel burn penalty

To evaluate the fuel burn penalty associated with a certain level of NO_x removal we estimate the increase in SFC (due to the pressure drop) and mass of the aircraft (due to the mass of the SCR catalyst, reductant carried and associated components such as reductant tanks and pumps). We do not consider other changes in mass, assuming they are relatively small and that the change in mass occurs relative to some future baseline design, *e.g.* a turbo-electric aircraft. Given an aircraft's range (R), flight speed (V), L/D, maximum landing mass (MLW), and the propulsion system's SFC, the Breguet range equation can be used to estimate cruise fuel burn.[31] To calculate the fuel burn for an aircraft with ammonia based SCR, the Breguet range equation needs to be modified, as detailed in the ESI,† to account for the consumption of the reductant during flight. For an aircraft with a given SFC, carrying and consuming fuel and reductant at the rate of $\dot{m}_f$ and $\dot{m}_{Red}$, respectively, the mass of fuel required is,

$$M_f = \frac{MLW}{1+\frac{\dot{m}_{Red}}{\dot{m}_f}}\left[\exp\left(\frac{SFC\left(1+\frac{\dot{m}_{Red}}{\dot{m}_f}\right)}{gR\frac{}{V\times L/D}}\right)-1\right]. \quad (2)$$

2.5 Modeling impacts of aviation emissions changes on global climate and air quality

The atmospheric chemistry and transport of various chemical species is calculated by using the GEOS-Chem global atmospheric chemistry-transport model (version 12.0.2).[32] The standard mechanism is employed, including tropospheric and stratospheric chemistry and physics.[33] The spatial resolution used is a $4^\circ \times 5^\circ$ global grid, with 72 non-uniform vertical layers (from sea-level up to a pressure of 1 Pa). The MERRA-2[34] meteorological data from the Global Modeling and Assimilation Office (GMAO) at NASA's Goddard Space Flight Center is used. GEOS-Chem solves global chemistry and transport equations to estimate the global atmospheric composition at 20 minute and 10 minute time steps respectively.

The baseline impact of aviation on radiative forcing and surface air quality is determined by performing two GEOS-Chem simulations, one with and one without aviation emissions for 2015, such that the differences in atmospheric composition between the two cases (after a spin up period of one year) are attributable to baseline aviation emissions. Similarly, the impact of post-combustion emissions control (PCEC) and ultra-low sulfur fuel (ULS) is the difference in atmospheric composition between simulations where aviation emissions are at their baseline values and simulations where the aviation emissions have been adjusted for a comparison scenario of fleet-wide use of PCEC with ULS fuel. The emissions are obtained by scaling down aviation NO_x emissions and introducing ammonia emissions (NH_3) to capture the effect of ammonia slip (any ammonia that remains un-reacted downstream of the catalyst) when PCEC is used. The fleet-wide application is not intended to be representative of an introduction scenario, but as with comparable analyses[22] to enable calculation of a representative average of the environmental impacts of PCEC. The effect of ULS fuel is modeled by reducing the fuel sulfur content from 600 ppm (typical jet fuel) to 15 ppm. The CO_2 emissions from the life-cycle of the fuel and ammonia (in the PCEC scenario) are also considered in the analysis.

Table 2 Emission inventories used in GEOS-Chem simulations

Region	Inventory	Species
Global	EDGARv43[40]	NO_x, SO_x, SO_4, CO, NH_3
Global	BOND[41]	BC, OC
Global	RETRO[42]	NMVOCs except C_2H_6 and C_3H_8
Global	SHIP[43]	NO_x, SO_2, CO
Global	ParaNOx[44]	O_3, HNO_3
Global	C2H6_2010[45]	C_2H_6
Global	POET[46]	C_2H_5OH
Asia	MIX[47]	NO_x, SO_2, CO, BC, OC, NMVOCs, NH_3
US	NEI2011[48]	NO_x, SO_2, CO, BC, OC, NMVOCs, NH_3
Canada	APEI[49]	NO_x, SO_x, CO, BC, OC, NMVOCs, NH_3
Mexico	BRAVO[50]	NO_x, SO_2, CO
Europe	EMEP[51]	NO_x, SO_2, CO
Global	VOLCANO	SO_2
Global	Lightning[52]	NO
Global	SoilNOx[53]	NO
Global	BROMOCARB[54]	$CHBr_3$, CH_2Br_2
Global	IODOCARB[55]	CH_3I, CH_2I_2, CH_2ICl, CH_2IBr
Global	MEGAN[56]	Biogenic hydrocarbons

The anthropogenic, biogenic, and natural emissions inventories in GEOS-Chem used for all scenarios are shown in Table 2. However, we note that the marginal benefits of NO_x reduction from aviation may be higher if a future cleaner atmosphere were used as the background.[35,36] Details of the aviation emissions inventory for each scenario considered, including life-cycle emissions are provided in Table 3. In the simulation year (2015) aviation emissions accounted for 2.1% of the global NO_x emissions from all sources compared to ~12% from lightning. If we consider the Northern Hemisphere above 1 km in altitude, aviation accounts for ~20% of all NO_x emissions, with the remainder being produced by lightning. NO_x emissions in this region are associated with increased ozone production and climate impacts relative to surface NO_x emissions.[37] The NO_x burden is provided in Section 3.7.

The well-to-tank emissions for conventional jet fuel and ULS fuel are taken from Stratton *et al.*[38] While the combustion CO_2 emissions of ULS fuel are lower (by ~0.4%) than conventional

Table 3 Aviation emissions scenarios considered in this work. Baseline aviation emissions used are from the Aviation Environmental Design Tool (AEDT) for the year 2015. Note that the PCEC scenario uses ULS fuel to prevent catalyst fouling. All emissions are quoted in teragrams per year (Tg per year)

	Baseline	ULS fuel	PCEC
Fuel burn	240	240	241
NO_2	3.60	3.60	0.175
SO_x	0.290	0.007	0.007
Combustion CO_2	757	754	758
Well-to-tank CO_2-eq.[38]	148	168	169
NH_3 life-cycle CO_2-eq.[39]	—	—	1.87

jet fuel, due to a change in the hydrogen to carbon ratio during the desulfurization process, the life-cycle CO_2 emissions (well-to-wake) from ULS fuel are ~2% higher than conventional jet fuel, which we account for.[22,38] The global average estimate of life cycle emissions for ammonia are taken from Bicer *et al.*[39]

2.5.1 Climate impacts due to post-combustion emissions control. The radiative forcing (RF) due to aviation emissions is estimated using the RRTMG (Rapid Radiative Transfer Model (Global)) integrated in GEOS-Chem. These RF values along with scenario specific emissions are then used in the Aviation Portfolio Management Tool – Impacts Climate v24 (AMPT IC)[57] to estimate the monetized climate related damages due to aviation emissions. APMT-IC is a simplified model that estimates the physical and economic impact of aviation on global climate including the associated uncertainties. The radiative forcing due to aviation is first translated into estimated changes in surface temperature. From this, we monetize the overall impact of aviation on the climate, which is discounted for future years and the total net present value (NPV) is reported.

In this work a single year of aviation emissions (for the year 2015) and its integrated impact into the future is considered. This is carried out for each scenario outlined in Table 3. While post-combustion emissions control may not be applicable in all aircraft, this analysis will allow future research to scale the benefits and costs based on the percentage of aviation fuel burn where post-combustion emissions control is practical. A discount rate of 3% is used to discount the damages occurring in the future and the NPV is used to compare the climate damages from the two scenarios.

2.5.2 Air quality related impacts of post-combustion emissions control. The population exposure to $PM_{2.5}$ and ozone is calculated by weighting the annual average ground level concentration with the global population density (using LandScan 2015 population distribution at a $0.1^\circ \times 0.1^\circ$ resolution).

The premature mortalities due to aviation attributable $PM_{2.5}$ and ozone are estimated using log-linear concentration response functions (CRF). The ozone impacts are estimated using the relative risk from Jerrett *et al.*[58] This study found a 4% [95% CI: 1.3% to 6.7%] increase in risk of respiratory disease related mortality per 10 ppbv increase in the daily 1 hour maximum ozone concentration (MDA1) during local ozone season. The health impacts due to $PM_{2.5}$ exposure are estimated using the relative risk from Hoek *et al.*[59] This meta-analysis of epidemiological studies reports a 11% [95% CI: 5.0% to 16%] increase in cardiovascular mortality rates per 10 mg increase in annual average $PM_{2.5}$ exposure.

An EPA-recommended[60] cessation lag of 20 years is used. It assumes that 30% of the premature mortalities occur in the first year, 50% of the mortalities in the next 4 years and the final 20% over the remaining 15 years. Consistent with the method used in AMPT-IC, a discount rate of 3% is used when monetizing impacts. The damages due to premature mortalities are calculated based on the US EPA estimates of the value of statistical life (VSL).[61] The resulting mean US VSL (scaled from 1990 income levels using an income elasticity of 0.7) is $10.2 million (in 2015 US dollars). The VSL for other countries is calculated from the US value using the gross domestic product per capita (PPP basis) and adjusted using an income elasticity of 0.7.[62]

3 Results and discussion

We obtain an estimate of the effectiveness of post-combustion emissions control for NO_x reduction in aircraft gas turbine engines. The results shown here are for a geared turbofan configuration (based on data provided by a major aero-gas turbine manufacturer) with the SCR catalyst installed downstream of the LPT. The core exhaust is assumed to be accelerated downstream of the catalyst in a propelling nozzle to produce thrust. However, we envision that the actual application of post-combustion emissions control with a clean-sheet engine and aircraft design may be configured so that all the thrust is delivered by separate propulsors. This may be in a turbo-electric configuration or by mechanical transmission.

3.1 Mass transfer limited regime

To verify that the catalyst is operating in the mass transfer limited regime we calculate the Damköhler number

$$\mathrm{Da} = \frac{k_c d}{D_{NO}},$$

where k_c is the rate constant for the chemical reaction[63] and D_{NO} is the diffusivity of NO at a particular temperature and pressure which is calculated based on Tang *et al.*[64] At temperatures of ~450 °C the catalytic reactions are confined to a 5–10 μm layer of the wash-coat.[13] We account for the effective diffusivity of the reactants using a porosity of ~0.56 and tortuosity factor of 2 per Beeckman.[65] The effective diffusion[66] is $D_{eff} = \theta \times D/\tau$, where θ is the porosity and τ is the tortuosity. Therefore, $D_{eff} = 0.56 \times D/2 \approx 0.3 \times D$.

At the temperatures and pressures found downstream of the LPT, we find $\mathrm{Da} \approx 1.6 \times 10^{10}$, which indicates that the chemical reactions are several orders of magnitude faster than the mass transfer from the free stream to the wall.

$DeNO_x$ is thus only dependent on the non-dimensional parameter $z^* = (zD_{NO})/(ud^2)$. Thus the required residence time ($\tau = z/u$) for a certain level of $deNO_x$ is dependent only on the square of the hydraulic diameter of the channel,

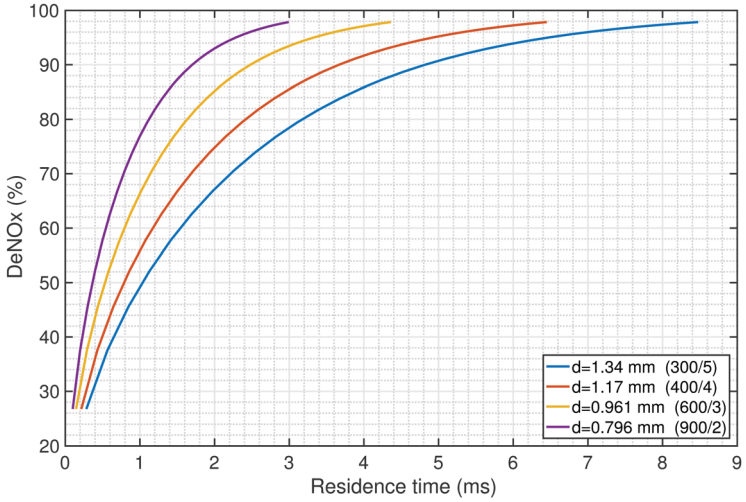

Fig. 3 DeNO$_x$ against τ for different channel hydraulic diameters. 300/5 refers to a catalyst substrate of 300 cells per square inch (cpsi) with a wall thickness of 0.127 mm (5 mil), which is the conventional way of characterizing the catalyst substrate geometry.

d^2 (for a given diffusivity D_{NO}). A smaller channel diameter implies a shorter residence time is required as compared to a larger channel diameter (see Fig. 3).

3.2 Estimating fuel specific reductant consumption

The fuel-specific reductant consumption (FSRC) for various reductants is calculated based on X_{m,NH_3} (moles of NH_3 per kg reductant) and an average cruise NO_x emissions index (EI(NO_x)) of 14 g kg^{-1}.[67] From the results in Table 1 we see that pure anhydrous liquid ammonia has the lowest reductant consumption as it has the highest ammonia content per unit mass. We note that post-combustion emissions control is also applicable to the landing and takeoff cycle, but here we first consider the cruise EI(NO_x) as this dominates NO_x emissions and corresponding reductant consumption.

The capacity of the reductant storage tank and hence the weight of the storage system is estimated using eqn (2). The total mass of fuel spent for a 1500 km range mission is approximately 4.1 tonnes, which would require 21 kg of anhydrous NH_3 to treat the NO_x emissions (based on the FSRC calculated in Table 1). Using the density of anhydrous liquid NH_3 the volume of the storage tank required is 35 L (9.25 gal). Storage tanks for anhydrous NH_3 are typically filled to ~85% of the total volume (~15% vapour space must be maintained to account for expansion).[68] Therefore for the design range the storage tank has a volume of ~42 L (cylindrical tank of inner radius of 15 cm and a length of 0.6 m) and is designed for a gauge pressure of 250 psi (~1725 kPa) (based on safety recommendations for ammonia storage[69]). This results in an empty tank weight of approximately 8 kg per aircraft. Anhydrous ammonia pumps for the required flow rates weigh approximately 60 kg[70] per engine. Assuming that any additional mass requirements for piping and injectors are small, we use 128 kg (a pump for each engine in a two-engine aircraft and a single NH_3 storage tank) as the total additional mass due to the reductant storage and delivery systems.

3.3 Effect of catalyst size on deNO$_x$ and fuel burn penalty

The effect of catalyst size on deNO$_x$ and the associated fuel burn penalty is shown in Fig. 4. The reacting length was fixed at 1.25 cm in this analysis as this results in a packed size that could fit in two of the typical seven containers of the cargo hold in an A320 aircraft.

The gas hourly space velocity (GHSV) is defined as the ratio of the volume flow rate per hour of the exhaust gas to the bulk volume of the catalyst and is inversely proportional to the residence time in the catalyst. A large catalyst corresponds to a smaller GHSV (longer residence time) and hence shows a greater conversion of NO_x. Fig. 4 shows that post-combustion emissions control as evaluated here has the potential to reduce the NO_x emissions by 95% in exchange for approximately a 0.5% increase in fuel burn. The catalyst total frontal area required for this conversion is approximately 19 m^2.

The deNO$_x$ at take-off conditions is approximately 75%. The lower NO_x conversion efficiency at take-off is due to the higher pressures at sea-level (relative to cruise altitude) which decreases the effective diffusivity (D_{eff}) of the reacting species by ~60% relative to cruise conditions. The increased NO_2 emission fraction at low thrust conditions (such as at idle conditions) does not affect the results because the conversion of NO_x is limited by the bulk mass transfer and not the chemical kinetics (Da $\gg$ 1).

Reduction in the conversion efficiency while the catalyst warms up has not been accounted for. In addition, the impact of the NO_x reduction across each flight segment, especially idle and taxi warrant further analysis with respect to local air quality.

The deNO$_x$ during cruise is higher (~97%) which results in an effective deNO$_x$ of ~95% over the full flight (a 1500 km range mission is assumed here). Furthermore, according to Yim *et al.*,[71] cruise emissions account for three-quarters of the premature mortalities attributable to aviation $PM_{2.5}$ and ozone. The design point of our catalyst is therefore chosen to be the

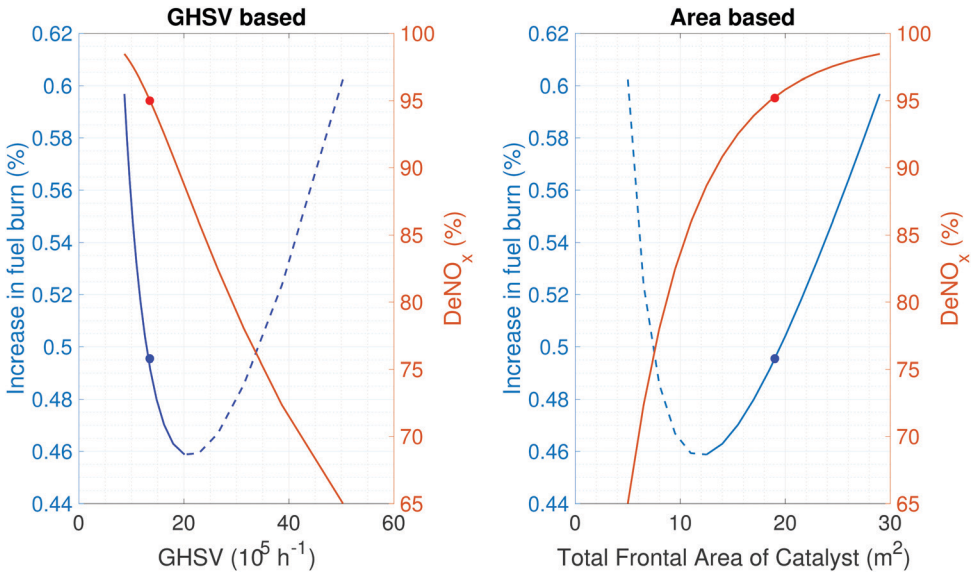

Fig. 4 Tradeoff between catalyst size and performance shown on two different basis. Left: Effect of GHSV on deNO$_x$ and fuel burn penalty. Right: Effect of flow through area on deNO$_x$ and fuel burn penalty. Chosen design point is marked with solid circles. Solid portion of the fuel burn curve represents the desirable region of operation where the catalyst efficiency is high, while the dashed portion of the curve represents the operating region where there is insufficient residence time for the catalyst to remove NO$_x$.

cruise condition, however to ensure catalyst performance at off-design conditions, we calculate the temperature of the gas entering the catalyst at take-off and idle to be ~480 and ~250 °C respectively which fall well within the operating range (150–600 °C)[17] of the zeolite class of substrates chosen in our analysis.

As the size of the catalyst is increased the pressure drop incurred can be reduced (decreasing fuel burn). However, this comes at the cost of additional weight (increasing fuel burn). This tradeoff is shown in the graph on the right in Fig. 4, as the frontal area of the catalyst is increased from approximately 5 m^2 to 10 m^2 the fuel burn penalty decreases. This is a consequence of the lower flow velocity and hence smaller pressure drop downstream of the LPT. Further increase in the flow through area results in an increase in fuel burn penalty. This is due to the catalyst mass, which affects the maximum landing mass of the aircraft and hence the fuel required to fly the same mission.

The dashed blue lines in Fig. 5 show that as the reacting length (l) is decreased for a fixed catalyst frontal area (A) the

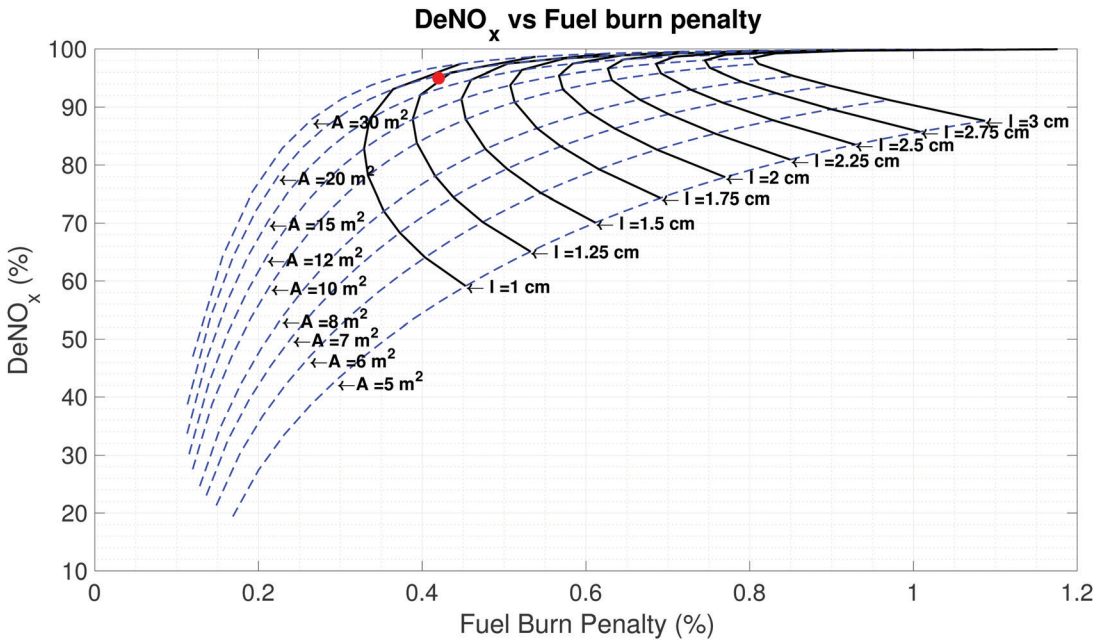

Fig. 5 Tradeoff between deNO$_x$ and fuel burn penalty. Each dashed blue lines show effect of changing reacting length (l) for a fixed frontal area (A). Solid black lines show the effect of changing frontal area while holding the reacting length constant. The design point is marked by red dot.

Table 4 Design values of the SCR system for the chosen design mission

Parameter	Value
NO_x reduction ($deNO_x$)	95%
Increase in fuel burn	0.5%
Catalyst frontal area	19 m^2
Reacting channel length	1.25 cm
Catalyst porosity	0.56
Catalyst tortuosity factor	2
Catalyst mass (per engine)	91 kg
Mass of reductant (for 1500 km mission)	21 kg
Additional system mass (pumps, storage tanks, *etc.* per aircraft)	128 kg
Pressure loss at cruise	115 Pa
Packed volume of catalyst	1.57 m^3

pressure drop and the catalyst volume (and hence catalyst mass) decrease. This causes the $deNO_x$ and fuel burn penalty to monotonically decrease. However, if l is held constant and A is increased, the pressure drop decreases but the catalyst mass increases. This causes the fuel burn penalty to first decrease and then increase as explained above. Higher lift to drag ratio airframes will mitigate the impact that this additional weight has on the fuel burn penalty, shifting the optimum. This is seen from the modified range equation (eqn (2)). Details of the SCR system at the chosen design point are outlined in Table 4.

3.4 Trade off between $deNO_x$, ammonia slip, and fuel burn penalty

Emissions of unreacted ammonia, referred to as ammonia slip, can be quantified using the stoichiometric ratio of the SCR reaction. In some designs, a catalyst is introduced downstream of the SCR to oxidize any unreacted ammonia in the exhaust stream. Catalyst designs have also been proposed where the monolith substrate is coated in layers of different catalytic materials which minimizes ammonia slip. For a reacting length of 1.25 cm and a total frontal area of 19 m^2 we calculate a 95% reduction in NO_x emissions for approximately a 0.5% increase in fuel burn. Calculating the average ammonia slip over the mission in terms of an emission index gives an $EI(NH_3)$ of approximately 0.26 g NH_3 per kg fuel.

While ammonia slip at ground level results in the formation of $PM_{2.5}$ which adversely affects human health,[1] cruise altitude emissions of ammonia do not share the same risk, since neither the ammonia nor its products would reach population at ground level due to wet deposition and atmospheric transport phenomenon at cruise altitude. However, we do include these emissions. The impact of ammonia slip is captured by the GEOS-Chem simulations as presented in Section 3.7. As identified by Eastham *et al.*[3] the transport of aviation attributable ozone from cruise altitude is the mechanism responsible for human exposure to both ozone and $PM_{2.5}$. This is supported by the analysis presented in Section 3.7.

3.5 Effect of engine core size on post-combustion emissions control

The 2016 report by the National Academies of Sciences, Engineering and Medicine on reducing global aviation carbon dioxide emissions[72] identifies small core engines as one of the high-priority research areas to reduce CO_2 emissions from commercial aviation. The NASA $N + 3$ aircraft concept design and trade studies final report[9] also outlines the interest in small core, high efficiency engines that are to be employed along with other configurations such as blended wing bodies, boundary layer ingestion and distributed propulsion.[9,26,30] We evaluate the impact that a small core engine architecture would have with regards to the use of post-combustion emissions control as outlined in this work.

Fig. 6 shows the results of evaluating the after-treatment methods on three different engine architectures. The conventional turbofan is representative of a modern mixed flow turbofan, the geared turbofan represents the state of the art low fan pressure ratio geared turbofans, and the small core engine is representative of an advanced engine architecture that was proposed to be used on the MIT D8 aircraft.[26]

We see from Fig. 6 that the performance of the post-combustion control system improves as the core size decreases. Considering the core size (expressed as the corrected mass flow at compressor exit), current generation engines have a core size of 3.18 kg s^{-1} (7 lb s^{-1}), geared turbofans have a core size of 2.27 kg s^{-1} (5 lb s^{-1}) and the next generation engines may have smaller core sizes of $\sim$0.68 kg s^{-1} (1.5 lb s^{-1}).[26] The thrust size for the conventional and geared turbofan engines is 110 kN (25 000 lbf) and the small core engine has the above core size is 58 kN (13 000 lbf). The small core engine has a lower thrust rating since the airframe envisioned by Lord *et al.*[26] (the MIT D8 design) has a higher L/D of approximately 20.[30]

The authors envision the proposed post-combustion emissions control methods could be implemented with a small core architecture that could be housed within the body of the aircraft in a turbo-electric configuration or possibly with a decoupled propulsor such as in the D8 aircraft.[26] This could allow installation of the catalyst in the fuselage of the aircraft. The core flow in such a design would thus contribute little or no thrust, although the design may be configured such that the core ingests the airframe boundary layer, providing scope for further improvement of the post-combustion emissions control performance.

3.6 Packing constraints and maintenance

The packaging of this catalyst into the airframe may not be possible with a "flat" catalyst configuration as shown in Fig. 2. An air-filter like pleated design allows us to pack a large area catalyst into a small packing volume. A schematic is shown in Fig. 7, where the flow enters axially and leaves radially. As shown in the supplementary information, a pleated design with internal radius r, pleat depth h, N pleats, reacting length l, and total length L, surface area of the interior is given by

$$A = 2NL\sqrt{h^2 + \frac{r^2}{2}(1 - \cos(2\pi/N)) - l^2}. \quad (3)$$

Applying eqn (3) shows that we can fit this area of catalyst into a cylinder of length 2.2 m and outer diameter of 1 m (using 24 pleats and a pleat depth of 18 cm). Detailed analysis concerning the packing and manufacturing of the catalyst design will be subject of future research.

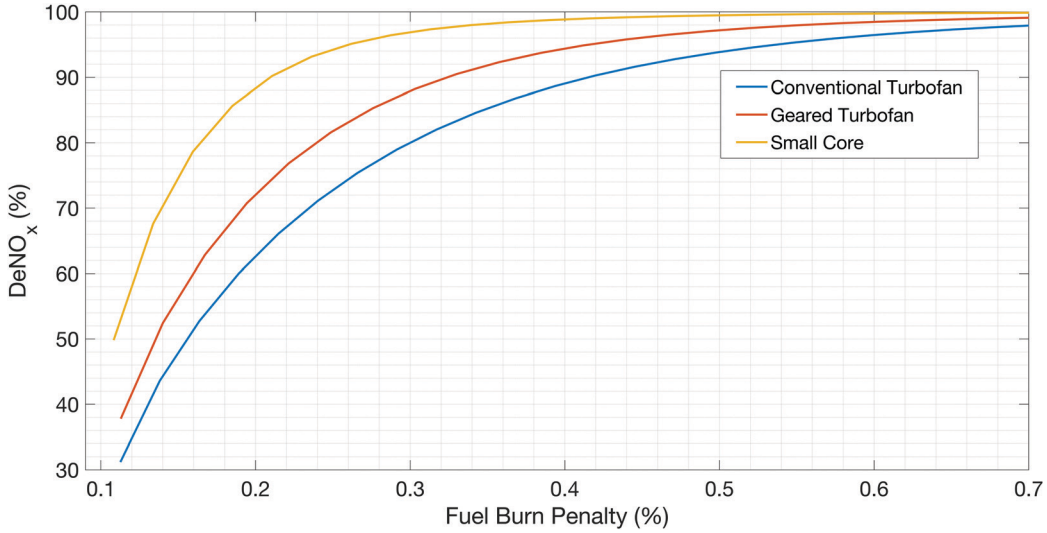

Fig. 6 Post-combustion emissions control applied to different engine architectures. As the core size (corrected mass flow at compressor exit) decreases from the conventional turbofan to the small core engine, higher NO_x reduction can be achieved for a smaller fuel burn penalty.

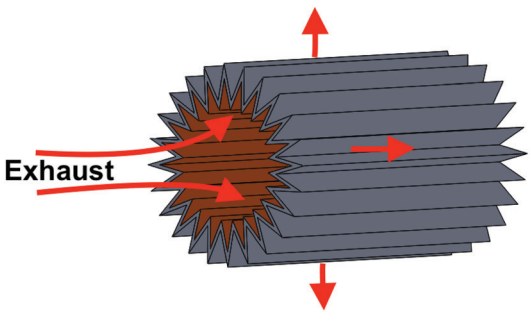

Fig. 7 Illustration of pleated catalyst design to pack large area catalyst into the fuselage.

The efficiency of the catalyst in removing NO_x from the exhaust decreases over time. The typical life time of a catalyst used in ground-based power plants is ~40 000–60 000 hours.[69] Assuming a similar life time for the catalyst used on board an aircraft and maintenance (C-check) intervals of ~7500 hours,[73] the catalyst will need to be replaced every 5–8 maintenance cycles.

3.7 Air quality impacts due to post-combustion emissions control

We use the GEOS-Chem global chemistry and transport model to estimate the air quality impacts of applying post-combustion emissions control to aviation.

We find that the contribution of global aviation to NO_x emissions while using post-combustion emissions control along with ULS fuel is approximately 0.11%, while the baseline contribution of aviation as outlined in Section 2.5 is ~2.1%. Furthermore, the combination of PCEC with ULS fuel reduces aviation's contribution to NO_x emissions in the free-troposphere of the Northern Hemisphere to 0.81% from a baseline of ~20%. Additionally, baseline aviation emissions are responsible for ~34% of the Northern Hemisphere NO_x mixing ratios at typical cruise altitudes (10–12 km) (*i.e.* zonally mass averaged across cruise altitudes and the Northern Hemisphere). The use of PCEC along with ULS fuel reduces the aviation attributable NO_x mixing ratio at Northern Hemisphere cruise altitudes to approximately 0.25% (see ESI† for further information).

3.7.1 Impact on $PM_{2.5}$ and ozone concentrations. The surface concentration of $PM_{2.5}$ and ozone attributable to aviation are shown in Fig. 8 and 9. The population weighted global annual average exposure to ozone and $PM_{2.5}$ are shown in Table 5.

Post-combustion emissions control along with desulfurized jet fuel leads to a reduction (87% from the baseline as defined in Table 3) in population exposure to $PM_{2.5}$ of which approximately 11% of the reduction in population exposure to $PM_{2.5}$ is due to the use of ULS fuel and the rest is attributable to the removal of NO_x. ULS fuel is required to prevent fouling of the catalyst as detailed in Section 1.2.4. The reduction in surface concentration of $PM_{2.5}$ is therefore primarily attributable to the post-combustion reduction of NO_x emissions. The global distribution of $PM_{2.5}$ and the reduction due to PCEC is shown in Fig. 8.

We find that using ULS fuel results in a reduction of sulfate aerosol in the lower stratosphere. This leads to a reduction in heterogeneous hydrolysis of N_2O_5 on sulfate aerosols and a subsequent reduction in ozone depletion by halogen catalysed cycles.[74] This increases the ozone concentration in the lower stratosphere and in stratospheric air masses that enter the troposphere, thereby resulting in an increase in the surface concentration of ozone as seen in Table 5. This finding is consistent with the findings by Eastham *et al.*[75]

Furthermore, the identified pathway implies that this effect will reduce in future years as the concentration of halogens in the atmosphere decreases (since the adoption of the Montreal Protocol).

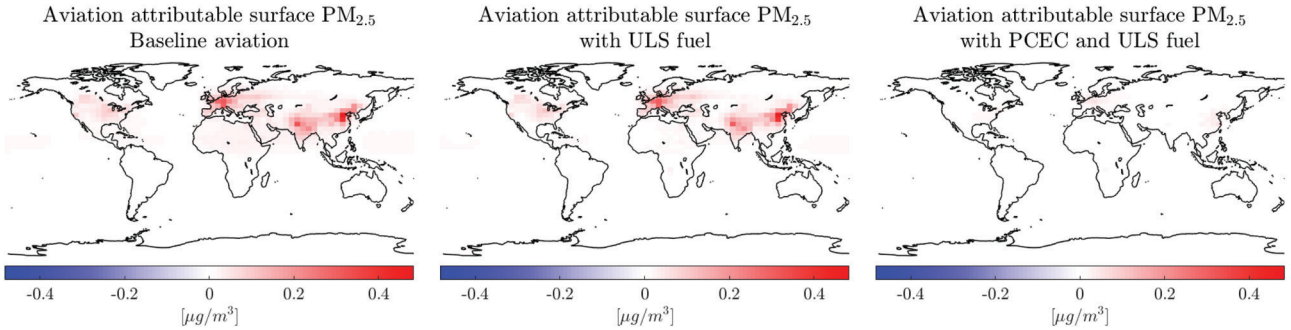

Fig. 8 Annual average ground level $PM_{2.5}$ concentration attributable to aviation in μg m^{-3}. Left: Baseline scenario. Centre: Aviation with ULS fuel. Right: Aviation with ULS fuel and post-combustion emissions control.

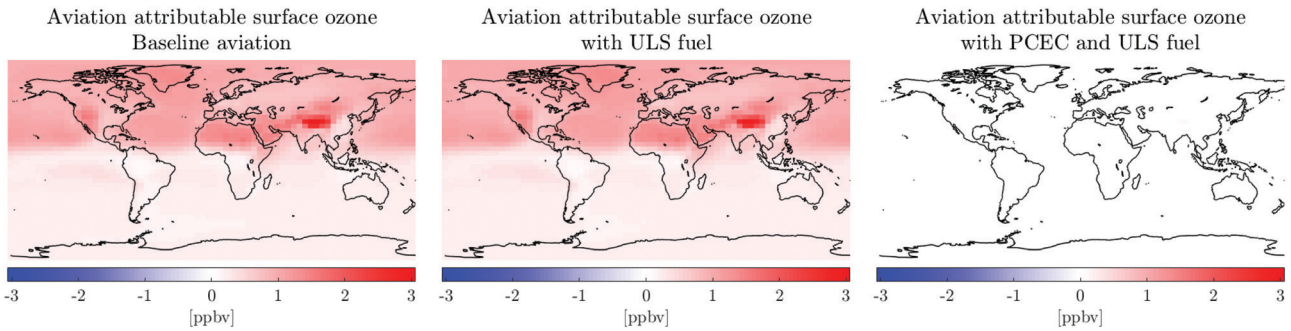

Fig. 9 Annual average ground level ozone concentration attributable to aviation in ppbv. Left: Baseline scenario. Centre: Aviation with ULS fuel. Right: Aviation with ULS fuel and post-combustion emissions control.

Table 5 Population weighted global, annual average exposure of $PM_{2.5}$ and ozone

Species	Δozone [ppbv]	$\Delta PM_{2.5}$ [μg m^{-3}]
Baseline aviation	0.640	0.0702
ULS	0.641	0.0625
PCEC with ULS	0.0223	0.00911

The average reduction in population exposure to ozone due to the use of post-combustion emissions control with ULS fuel is 97%. The reduction in surface ozone concentration is a consequence of the reduced NO_x emissions due to post-combustion control through the mechanism described by Eastham *et al.*[3]

While reducing ground level ozone concentration has a health benefit, a reduction in column ozone can increase the risk of melanoma. However as estimated by Eastham *et al.*[3] the avoided mortalities due to melanoma resulting from column ozone created by aviation is small (2.5%) compared to the $PM_{2.5}$ and ozone related air quality impacts attributable to aviation.

3.7.2 Premature mortalities avoided through post-combustion emissions control. We estimate that the total premature mortalities due to aviation emissions is ∼24 000 globally [95% CI: 14 000 to 34 000]. Of this the premature mortalities due to aviation attributable $PM_{2.5}$ is ∼15 000 [95% CI: 7300 to 22 000]. An additional 8900 [95% CI: 2900 to 15 000] premature mortalities are due to an increased exposure to ozone.

These baseline values are consistent with previous estimates of aviation attributable premature mortalities [3] when accounting for the addition of new emission inventories in GEOS-Chem and the increase in aviation fuel burn by ∼30% (188 Tg in the AEDT-2005 inventory *vs.* 240 Tg in the AEDT-2015 inventory). The $PM_{2.5}$ and ozone attributable premature mortalities in each of the scenarios outlined in Table 3 are shown in Fig. 10.

Post-combustion emissions control used with ULS jet fuel (PCEC-ULS), decreases the population exposure to $PM_{2.5}$ and ozone by reducing NO_x and SO_x emissions. Converting

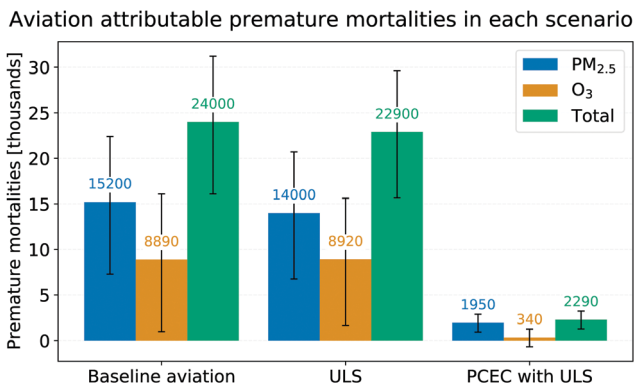

Fig. 10 Premature mortalities attributable to aviation under the scenarios considered. The error bars shown are the 95% confidence intervals from the Monte Carlo runs.

exposure to mortality using the concentration response functions described earlier, we estimate that ~13 000 premature mortalities (95% CI: 6300 to 19 000) due to exposure to $PM_{2.5}$ and ~8500 premature mortalities (95% CI: 2800 to 14 000) due to exposure to ozone are avoided by using PCEC and ULS fuel. Furthermore, ~12 000 (95% CI: 5900 to 18 000) of the ~13 000 avoided premature mortalities due to decreased exposure to $PM_{2.5}$ are attributable to the post-combustion removal of NO_x emissions while the remaining avoided premature mortalities are attributable to reduced $PM_{2.5}$ from the use of ULS fuel (see Section 2.5).

Therefore ~22 000 [95% CI: 13 000 to 31 000] total premature mortalities are avoided due to the use of PCEC with ULS fuel annually. This is approximately 92% of all premature mortalities attributable to aviation as calculated in this study. The air quality benefits of using PCEC-ULS are monetized as described in Section 2.5.2. The benefit associated with the averted premature mortalities by using PCEC (with ULS fuel), amounts to approximately 77 billion USD (2015) annually [95% CI: 45 to 110 billion USD], or $320 per tonne of fuel burned.

3.8 Climate impacts due to post-combustion emissions control

The change in RF due to aviation emissions as estimated by RRTMG is shown in Table 6. We use RRTMG to estimate RF for tropospheric nitrates, sulfates and black carbon. Ozone RF is quantified in APMT, using an approach which accounts for both short-term and long-term ozone responses.

The lower sulfate concentration when ULS fuel is used, reduces competition for available ammonium resulting in an increase in nitrate formation and therefore an increased cooling effect from nitrates in the ULS scenario as seen in Table 6. The changes in black carbon RF are negligible. The values of radiative forcing from Table 6 are used in APMT-IC to estimate the climate damages due to aviation.

Table 6 Change in net (shortwave + longwave) all-sky radiative forcing due to aviation emissions as estimated by the RRTMG module in GEOS-Chem in mW m^{-2}. The baseline column shows the change in RF due to global aviation without the use of any post-combustion emissions control

	Baseline aviation	ULS	PCEC with ULS
Sulfates	−6.21	−1.41	−0.114
Nitrates	−0.667	−1.83	−0.387
Black carbon	0.537	0.534	0.568

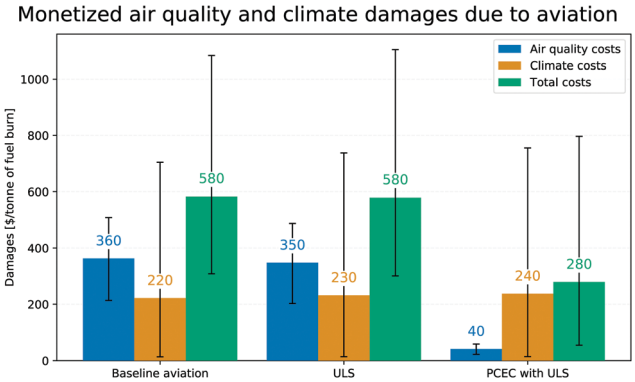

Fig. 11 Air quality (AQ), climate and total cost per tonne of fuel burnt in each of the scenarios considered. Post-combustion removal of NO_x together with the use of ULS fuel results in ~89% reduction in air quality costs and a ~9% increase in climate costs per tonne of fuel burn compared to the baseline scenario. Values are in 2015 US dollars per tonne of fuel burn. Error bars shown are the 95% confidence intervals of the Monte Carlo runs.

The total climate damages associated with ULS fuel and post-combustion emissions control is estimated using APMT-IC to be approximately 57 billion USD (or $238 per tonne of fuel burned) compared to a baseline climate damage of 53 billion USD (or $222 per tonne of fuel burned) due to global aviation without post-combustion emissions control. These damages include the life cycle emissions of CO_2 as detailed in Table 7. Therefore the use of PCEC with ULS fuel results in a ~7.5% increase in climate damages from all aviation. As seen in Table 7 the dominant contribution is from the decreased cooling effect due to a lower sulfate aerosol concentration when ULS fuel is used. The increase in climate damages due to an increase in fuel burn (~0.5%) as a result of the additional weight and pressure losses introduced by the PCEC system is partially offset by the lower combustion CO_2 emissions from the ULS fuel used[22,38] as seen in Table 7.

The net benefit (*i.e.* the monetized benefit due to avoided premature mortalities less the increase in climate damages) is therefore approximately 73 billion USD annually [95% CI: 40 to 100 billion USD] or a mean value of $304 per ton of jet fuel burnt. The environmental costs normalized by fuel burn (from degraded air quality and climate related damages) are shown in Fig. 11. The baseline costs are consistent with recent work by Grobler *et al.*[76]

Table 7 APMT-IC derived mean climate damages. All values are in billions of 2015 USD. Negative values of damage indicate a benefit. The life cycle CO_2 costs are given for a well to wake emissions of CO_2

	Baseline	ULS	PCEC with ULS
Life cycle CO_2 (of which combustion CO_2)	40.4 (33.7)	41.0 (33.5)	41.3 (33.7)
NO_x	−1.02	−1.43	−0.175
Sulfates	−2.19	−0.0120	−0.00100
Black carbon	0.190	0.189	0.201
Total cost[a]	53.2	55.6	57.2

[a] Note that the total cost includes life cycle CO_2 and consists of other short-lived forcers that are not shown in the table.

4 Conclusions

This work is the first proposal and assessment of post-combustion emissions control techniques for aircraft gas turbine engines and evaluates the case for the use of selective catalytic reduction for NO_x control in the aviation sector. The analytical approach, developed based on prior work done in SCR applications for diesel engines shows that a 95% reduction in NO_x emissions can be achieved for approximately a 0.5% increase in fuel burn. The sensitivity of the fuel burn to catalyst mass and catalyst induced pressure drop show that the performance of the emissions control system improves for future designs where smaller core sizes, higher engine efficiency and higher *L*/*D* airframes are expected. Furthermore optimization and improvements in catalyst technology will further improve the performance of post-combustion emissions control.

The current work quantifies the impact that a fleet-wide adoption of post-combustion emissions control will have on air quality and climate. However, the size requirements of the SCR system, particularly of the catalyst, imply that they will have to be housed within the aircraft fuselage, making this unsuitable for certain classes of aircraft. Post-combustion emissions control systems might be better suited for a hybrid- or turbo-electric design with small core engines. A NASA $N + 3$ aircraft design such as the D8 with small core engines, and turbo-electric designs, may offer further potential for optimization. Additionally using post-combustion emissions control to reduce NO_x could result in combustor design space benefits that improve combustor efficiency. Further analysis is required to quantify the performance of such an integrated aircraft system. The spatial distribution of aviation hubs and missions flown by aircraft where PCEC is feasible might result in spatial variations of the impacts, which also need to be quantified. Since the implementation cost of post-combustion emissions control technology is dependent on the aircraft configuration and specific design concepts, we do not include the cost of implementation in this analysis. However we estimate that the increase in annual fleet-wide operating cost due to the increased fuel burn (of $\sim$1.30 Tg per year) is approximately 875 million USD based on average price of \$86 per bbl for Jet-A.[77]

Using GEOS-Chem it is estimated that approximately 87% of surface $PM_{2.5}$ concentration and 97% of ozone concentration due aviation emissions is averted with the use of post-combustion emissions control with desulfurized jet fuel (as is required for PCEC) for a fleet-wide implementation (as a hypothetical analysis scenario). An analysis based on epidemiological studies shows that $\sim$22 000 premature mortalities are avoided ($\sim$92% of all premature mortalities attributable to aviation) due to exposure to $PM_{2.5}$ and ozone, if post-combustion emissions control is used along with ULS jet fuel. The mean monetized air quality benefits due to this is estimated to be \$77 billion annually. The increase climate damages associated with the use of post-combustion emissions control is estimated using APMT-IC to be \$4 billion annually. An environmental cost-benefit analysis, therefore, indicates that the net benefit of post-combustion emissions control is approximately \$73 billion annually or \$304 per ton of jet fuel burned.

Conflicts of interest

There are no conflicts to declare.

Acknowledgements

The authors would like to acknowledge the informative discussions with Professor Wai Cheng from the Sloan Automotive Laboratory and Dr Justin Kamp from the Department of Chemical Engineering at the Massachusetts Institute of Technology. We would also like to thank Pratt and Whitney for providing representative engine models to perform this study.

References

1 D. W. Dockery, C. A. Pope, X. Xu, J. D. Spengler, J. H. Ware, M. E. Fay, B. G. Ferris and F. E. Speizer, *N. Engl. J. Med.*, 1993, **329**, 1753–1759.
2 M. Kampa and E. Castanas, *Environ. Pollut.*, 2008, **151**, 362–367.
3 S. D. Eastham and S. R. H. Barrett, *Atmos. Environ.*, 2016, **144**, 17–23.
4 Boeing Commercial Airplanes Market Analysis, *Current Market Outlook 2016–2035*, 2016, www.boeing.com/cmo.
5 C. S. Dorbian, P. J. Wolfe and I. A. Waitz, *Atmos. Environ.*, 2011, **45**, 2750–2759.
6 H. Cohen, G. F. C. Rogers and H. I. H. Saravanamuttoo, *Gas Turbine Theory*, Longman Pub Group, 1996.
7 A. H. Lefebvre, *Int. J. Turbo Jet-Engines*, 1986, **21**, 231–243.
8 T. C. Lieuwen and V. Yang, *Gas Turbine Emissions*, Cambridge University Press, 2013.
9 E. M. Greitzer, P. A. Bonnefoy, E. D. L. R. Blanco, C. S. Dorbian, M. Drela, D. K. Hall, R. J. Hansman, J. I. Hileman, R. H. Liebeck, J. Lovegren, P. Mody, J. A. Pertuze, S. Sato, Z. S. Spakovszky, C. S. Tan and J. S. Hollman, *N + 3 Aircraft Concept Designs and Trade Studies, Final Report Volume 1*, 2010, https://ntrs.nasa.gov/archive/nasa/casi.ntrs.nasa.gov/20100042401.pdf.
10 A. Lefebvre, *Gas Turbine Combustion*, Taylor & Francis, 1983.
11 ed. H. Jääskeläinen and M. K. Khair, *DieselNet Technology Guide: Diesel Engines*, 2013, https://www.dieselnet.com/tech/diesel_engines.php.
12 T. V. Johnson, *Urea-SCR Technology for deNOx After Treatment of Diesel Exhausts*, Springer, New York, 2014, pp. 3–31.
13 M. Koebel, M. Elsener and M. Kleemann, *Catal. Today*, 2000, **59**, 335–345.
14 E. Tronconi and A. Beretta, *Catal. Today*, 1999, **52**, 249–258.
15 M. J. Moore, *Proc. Inst. Mech. Eng., Part A*, 1997, **211**, 43–52.
16 M. T. Timko, S. C. Herndon, E. C. Wood, T. B. Onasch, M. J. Northway, J. T. Jayne, M. R. Canagaratna, R. C. Miake-Lye and W. B. Knighton, *J. Eng. Gas Turbines Power*, 2010, **132**, 061504.
17 W. A. Majewski, *DieselNet Technology Guide: Diesel Catalysts*, 2005, http://www.dieselnet.com/tech/cat_scr.php.
18 W. A. Majewski and H. E. Jääskeläinen, *DieselNet Technology Guide: Catalytic Coating & Materials*, 2005, https://www.dieselnet.com/tech/cat_mat.php.

19 J. Wiehl and C. D. Vogt, *MTZ Worldwide*, 2003, **64**, 8–11.
20 G. Fulks, G. B. Fisher, K. Rahmoeller, M.-C. Wu, E. D'Herde and J. Tan, *SAE Technical Paper*, 2009.
21 *Environmental Protection Agency Control of Air Pollution From New Motor Vehicles: Heavy-Duty Engine and Vehicle Standards and Highway Diesel Fuel Sulfur Control Requirements*, 12, 2001.
22 S. R. H. Barrett, S. H. L. Yim, C. K. Gilmore, L. T. Murray, S. R. Kuhn, A. P. K. Tai, R. M. Yantosca, D. W. Byun, F. Ngan, X. Li, J. I. Levy, A. Ashok, J. Koo, H. M. Wong, O. Dessens, S. Balasubramanian, G. G. Fleming, M. N. Pearlson, C. Wollersheim, R. Malina, S. Arunachalam, F. S. Binkowski, E. M. Leibensperger, D. J. Jacob, J. I. Hileman and I. A. Waitz, *Environ. Sci. Technol.*, 2012, **46**, 4275–4282.
23 A. F. El-Sayed, *Aircraft Propulsion and Gas Turbine Engines*, CRC Press, 2nd edn, 2017.
24 *Paccar MX13 Engine Specifications*, https://paccarpowertrain.com/MX-13-Spec-Sheet.pdf.
25 M. P. Harold and P. Metkar, *Urea-SCR Technology for deNOx After Treatment of Diesel Exhausts*, Springer, New York, 2014, pp. 311–356.
26 W. K. Lord, G. Suciu, J. Chandler and K. Hasel, *53rd AIAA Aerospace Sciences Meeting*, 2015.
27 W. A. Majewski, *DieselNet Technology Guide: Catalyst Fundamentals*, 2000, https://www.dieselnet.com/tech/cat_fund.php.
28 E. Tronconi and P. Forzatti, *AIChE J.*, 1992, **38**, 201–210.
29 W. A. Majewski and H. E. Jääskeläinen, *DieselNet Technology Guide: Cellular Monolith Substrates*, 1998, https://www.dieselnet.com/tech/cat_substrate.php.
30 M. Drela, 29th AIAA Applied Aerodynamics Conference, 2011, 27–30.
31 J. Anderson, *Introduction to Flight*, McGraw-Hill Higher Education, 2015.
32 I. Bey, D. J. Jacob, R. M. Yantosca, J. A. Logan, B. D. Field, A. M. Fiore, Q. Li, H. Y. Liu, L. J. Mickley and M. G. Schultz, *J. Geophys. Res.: Atmos.*, 2001, **106**, 23073–23095.
33 S. D. Eastham, D. K. Weisenstein and S. R. Barrett, *Atmos. Environ.*, 2014, **89**, 52–63.
34 R. Gelaro, W. McCarty, M. J. Suárez, R. Todling, A. Molod, L. Takacs, C. A. Randles, A. Darmenov, M. G. Bosilovich, R. Reichle, K. Wargan, L. Coy, R. Cullather, C. Draper, S. Akella, V. Buchard, A. Conaty, A. M. da Silva, W. Gu, G.-K. Kim, R. Koster, R. Lucchesi, D. Merkova, J. E. Nielsen, G. Partyka, S. Pawson, W. Putman, M. Rienecker, S. D. Schubert, M. Sienkiewicz and B. Zhao, *J. Clim.*, 2017, **30**, 5419–5454.
35 C. K. Gilmore, S. R. Barrett, J. Koo and Q. Wang, *Environ. Res. Lett.*, 2013, **8**(3), 034027.
36 M. Woody, B. Haeng Baek, Z. Adelman, M. Omary, Y. Fat Lam, J. Jason West and S. Arunachalam, *Atmos. Environ.*, 2011, **45**, 3424–3433.
37 K. Dahlmann, V. Grewe, M. Ponater and S. Matthes, *Atmos. Environ.*, 2011, **45**, 2860–2868.
38 R. Stratton, H. Wong and J. Hileman, *Life cycle greenhouse gas emissions from alternative jet fuels*, 2010.
39 Y. Bicer, I. Dincer, C. Zamfierescu, G. Vezina and F. Raso, *J. Cleaner Prod.*, 2016, **135**, 1379–1395.
40 European Commission, Joint Research Centre (JRC)/Netherlands Environmental Assessment Agency (PBL), Emission Database for Global Atmospheric Research (EDGAR), 2011, http://edgar.jrc.ec.europa.eu, Release version 4.2.
41 T. C. Bond, E. Bhardwaj, R. Dong, R. Jogani, S. Jung, C. Roden, D. G. Streets and N. M. Trautmann, *Global Biogeochem. Cycles*, 2007, **21**(2), DOI: 10.1029/2006GB002840.
42 M. G. Schultz, A. Heil, J. J. Hoelzemann, A. Spessa, K. Thonicke, J. G. Goldammer, A. C. Held, J. M. C. Pereira and M. van het Bolscher, *Global Biogeochem. Cycles*, 2008, **22**(2), DOI: 10.1029/2007GB003031.
43 C. Wang, J. J. Corbett and J. Firestone, *Environ. Sci. Technol.*, 2008, **42**, 193–199.
44 G. C. M. Vinken, K. F. Boersma, D. J. Jacob and E. W. Meijer, *Atmos. Chem. Phys.*, 2011, **11**, 11707–11722.
45 Z. A. Tzompa-Sosa, E. Mahieu, B. Franco, C. A. Keller, A. J. Turner, D. Helmig, A. Fried, D. Richter, P. Weibring, J. Walega, T. I. Yacovitch, S. C. Herndon, D. R. Blake, F. Hase, J. W. Hannigan, S. Conway, K. Strong, M. Schneider and E. V. Fischer, *J. Geophys. Res.: Atmos.*, 2017, **122**, 2493–2512.
46 D. B. Millet, A. Guenther, D. A. Siegel, N. B. Nelson, H. B. Singh, J. A. de Gouw, C. Warneke, J. Williams, G. Eerdekens, V. Sinha, T. Karl, F. Flocke, E. Apel, D. D. Riemer, P. I. Palmer and M. Barkley, *Atmos. Chem. Phys.*, 2010, **10**, 3405–3425.
47 M. Li, Q. Zhang, J. Kurokawa, J.-H. Woo, K. B. He, Z. Lu, T. Ohara, Y. Song, D. G. Streets, G. R. Carmichael, Y. F. Cheng, C. P. Hong, H. Huo, X. J. Jiang, S. C. Kang, F. Liu, H. Su and B. Zheng, *Atmos. Chem. Phys. Discuss.*, 2015, **15**, 34813–34869.
48 H. Simon, L. Beck, P. V. Bhave, F. Divita, Y. Hsu, D. Luecken, J. D. Mobley, G. A. Pouliot, A. Reff, G. Sarwar and M. Strum, *Atmos. Pollut. Res.*, 2010, **1**, 196–206.
49 Air Pollutant Emission Inventory (APEI) Historical Trends – Open Government Portal, https://open.canada.ca/data/en/dataset/fa1c88a8-bf78-4fcb-9c1e-2a5534b92131, (Accessed on 01/29/2019).
50 H. Kuhns, M. Green and V. Etyemezian, *BRAVO Technical Steering Committee*, 2001.
51 M. Auvray and I. Bey, *J. Geophys. Res.: Atmos.*, 2005, **110**, D11303.
52 L. T. Murray, D. J. Jacob, J. A. Logan, R. C. Hudman and W. J. Koshak, *J. Geophys. Res.: Atmos.*, 2012, **117**, D20307.
53 R. C. Hudman, N. E. Moore, A. K. Mebust, R. V. Martin, A. R. Russell, L. C. Valin and R. C. Cohen, *Atmos. Chem. Phys.*, 2012, **12**, 7779–7795.
54 Q. Liang, R. S. Stolarski, S. R. Kawa, J. E. Nielsen, A. R. Douglass, J. M. Rodriguez, D. R. Blake, E. L. Atlas and L. E. Ott, *Atmos. Chem. Phys.*, 2010, **10**, 2269–2286.
55 C. Ordóñez, J.-F. Lamarque, S. Tilmes, D. E. Kinnison, E. L. Atlas, D. R. Blake, G. S. Santos, G. Brasseur and A. Saiz-Lopez, *Atmos. Chem. Phys.*, 2012, **12**, 1423–1447.
56 A. B. Guenther, X. Jiang, C. L. Heald, T. Sakulyanontvittaya, T. Duhl, L. K. Emmons and X. Wang, *Geosci. Model Dev.*, 2012, **5**, 1471–1492.
57 K. Marais, S. P. Lukachko, M. Jun, A. Mahashabde and I. A. Waitz, *Meteorol. Z.*, 2008, **17**, 157–172.

58 M. Jerrett, R. T. Burnett, C. A. Pope, K. Ito, G. Thurston, D. Krewski, Y. Shi, E. Calle and M. Thun, *N. Engl. J. Med.*, 2009, **360**, 1085–1095.
59 G. Hoek, R. M. Krishnan, R. Beelen, A. Peters, B. Ostro, B. Brunekreef and J. D. Kaufman, *Environ. Health*, 2013, **12**, 43.
60 T. Cameron and B. Ostro, Washington, DC, Science Advisory Board, 2004.
61 Guidelines for Preparing Economic Analysis (2010, revised 2014), 2014, https://www.epa.gov/environmental-economics/guidelines-preparing-economic-analysis-2010-revised-2014, (Accessed on 01/29/2019).
62 L. A. Robinson and J. K. Hammitt, The effect of income on the value of mortality and morbidity risk reductions. Recommended Income Elasticity and Income Growth Estimates: Technical Memorandum, 2016, https://yosemite.epa.gov/sab/SABPRODUCT.NSF/81e39f4c09954fcb85256ead006be86e/0CA9E925C9A702F285257F380050C842/File/Income+Elasticity+Technical+Memorandum_final_2_5_16_docx.pdf, (Accessed on 01/29/2019).
63 E. Tronconi, *Catal. Today*, 1997, **34**, 421–427.
64 M. J. Tang, R. A. Cox and M. Kalberer, *Atmos. Chem. Phys.*, 2014, **14**, 9233–9247.
65 J. W. Beeckman, *Ind. Eng. Chem. Res.*, 1991, **30**, 428–430.
66 C. N. Satterfield, *Mass Transfer Heterogeneous Catalysis*, MIT Press, Cambridge, MA and London, England, 1970.
67 ICAO Aircraft Engine Emissions Databank, 2017, http://www.easa.europa.eu/document-library/icao-aircraft-engine-emissions-databank, Version 24.
68 Storage and handling of anhydrous ammonia, 2011, https://www.osha.gov/laws-regs/regulations/standardnumber/1910/1910.111.
69 Cost Reports and Guidance for Air Pollution Regulations, 2019, https://www.epa.gov/economic-and-cost-analysis-air-pollution-regulations/cost-reports-and-guidance-air-pollution.
70 Blackmer NH3/LPG Pump, 3″-Dultmeier Sales, https://www.dultmeier.com/products/0.851.2042/11668#.
71 S. H. L. Yim, G. L. Lee, I. H. Lee, F. Allroggen, A. Ashok, F. Caiazzo, S. D. Eastham, R. Malina and S. R. H. Barrett, *Environ. Res. Lett.*, 2015, **10**, 034001.
72 Committee on Propulsion and Energy Systems to Reduce Commercial Aviation Carbon Emissions, *Commercial Aircraft Propulsion and Energy Systems Research*, National Academies Press, Washington, DC, 2016.
73 MRO Management, *Extension Lead*, 2017, http://www.mromanagement.com/feature/airbus-to-publish-a320neo-maintenance-tasks.
74 J. H. Seinfeld and P. N. Spyros, *Atmospheric chemistry and physics: from air pollution to climate change*, John Wiley & Sons, Hoboken, New Jersey, 1998.
75 S. D. Eastham, D. K. Weisenstein, D. W. Keith and S. R. Barrett, *Atmos. Environ.*, 2018, **187**, 424–434.
76 C. Grobler, P. J. Wolfe, K. Dasadhikari, I. C. Dedoussi, F. Allroggen, R. L. Speth, S. D. Eastham, A. Agarwal, M. D. Staples, J. Sabnis and S. R. H. Barrett, *Environ. Res. Lett.*, 2019, **14**, 114031.
77 Jet Fuel Price Monitor, https://www.iata.org/publications/economics/fuel-monitor/Pages/index.aspx, (Accessed on 01/29/2019).

